POLITECNICO DI TORINO

Collegio di Ingegneria Chimica e dei Materiali

Master of Science Course
in Materials Engineering

Master of Science Thesis

Thiol-ene biobased networks: Furan allyl derivatives for green coating applications

Supervisor:
Prof. Marco Sangermano

Candidate:
Dumitru Moraru

October 2023

Declaration

I hereby declare that the contents and organization of this thesis constitute my own original work and does not compromise in any way the rights of third parties, including those relating to the security of personal data.

Dumitru Moraru

2023

To my mother and in loving memory of grandfather

Abstract

The employment of biomass feedstocks is crucial in the development of sustainable materials as alternatives to fossil-based resources. Within this context, furan derivatives from hemicellulose have been investigated as viable bio-based building blocks. In our study, we focused on two specific furan derivatives, namely 2,5-Furandimethanol (FDM) and cis-cyclobutane-1,2-dicarboxylic acid (CBDA-2), which were derived from Furylacrylic acid. The allylation of these two compounds was carried out by a Ph.D student. The resulting bis-allyl derivatives were combined with commercially available tris- and tetra-functional thiol monomers then cured using UV light through a thiol-ene reaction. The UV-curing process was thoroughly studied using real-time FT-IR, photo-DSC, and photo-rheology techniques to investigate the curing kinetic. Subsequently, the bio-based thermosets were characterized using DMTA, DSC and tensile techniques to evaluate their thermal-mechanical behaviour. Furthermore, gel content, contact angle and hardness were assessed. The results demonstrated comparable properties to already studied bio-based thiol-ene thermosets, indicating the potential use of the studied material for coating applications.

Contents

List of Figures

List of Tables

Chapter 1

Introduction

The transition from fossil-based materials to bio-based alternatives poses a significant challenge for polymer scientists and industry. In the pursuit of more cost-effective and sustainable products, extensive research has explored renewable monomers such as sugars, polysaccharides, vegetable oils, lignocellulosic derivatives, pine resin derivatives, and proteins as precursors for polymers.

Renewable resources offer a diverse range of molecules and macromolecules produced through natural biological processes fuelled by solar energy. The utilization of lignocellulosic biomass, the most abundant and renewable biomass on Earth, shows potential as an alternative to fossil resources, with over 200 value-added compounds derived from it.[1]

Bio-based monomers, particularly those derived from lignocellulosic sources and byproducts of the food industry, are seen as promising replacements for petroleum-based counterparts.

Governments worldwide support the shift towards bio-based materials, aiming to increase their share as chemical and material sources. The exploration of plant biomass and the utilization of byproducts from industries like pulp and paper offers opportunities for sustainable material development.

In the quest for sustainable materials as alternatives to fossil-based resources we focused our work on exploring furan derivatives as viable bio-based building blocks from lignocellulosic biomass.[2] The aim of this study is to characterize a bio-based thiol-ene moiety for coating applications by using allylated compounds derived from cellulose and hemicellulose building blocks. The coating was obtained using UV-curing technology, aiming to minimize environmental impact by reducing energy consumption and shortening reaction time, compared to conventional thermal methods.[3,4] Figure 1 illustrates the different constituents that contribute to the extensive intramolecular and intermolecular hydrogen bonding networks found in lignocellulosic biomass[1].

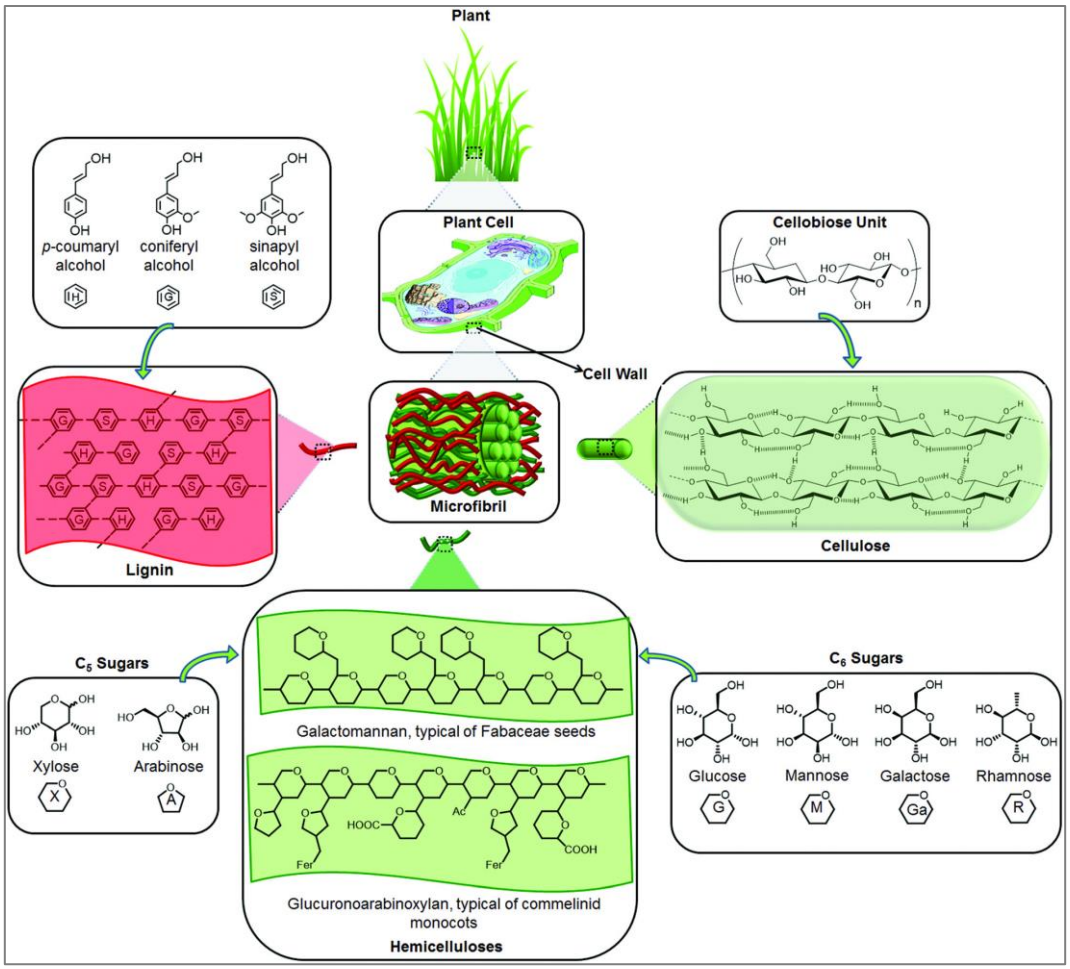

Figure 1: The main components of lignocellulose.[1]

Specifically, we directed our attention to two furan derivatives, namely 2,5-Furandimethanol (FDM) and cis-cyclobutane-1,2-dicarboxylic acid (CBDA), which were derived from Furylacrylic acid by allylation of cellulose and hemicellulose compounds. The resulting bis-allyl derivatives were then combined with commercially available tris- and tetra-functional thiol compounds and subjected to UV light-induced curing through a thiol-ene reaction.

Subsequently the obtained samples were characterized.

1.1 Photo-polymerization process

By photopolymerization we mean a chemical reaction that occurs when a liquid substance, called a prepolymer, undergoes polymerization upon exposure to light via chemical bond formation and a conversion to a solid state is achieved. It is a process in which the monomer or oligomer molecules combine with each other to form larger polymer chains or networks, in presence of other reagents.

The moiety is entirely composed of reactive material and typically comprises the following components:

- prepolymer (or oligomers)
- diluents (or monomers)
- photo-initiator (PI)
- co-initiator, chain transfer agent
- light stabiliser
- thermal stabiliser
- colourants, plasticisers, and additives.

The first three components can be found in nearly all formulations.[5]

The reaction is initiated by a photochemical initiator, also known as a photo-initiator (PI). These initiators absorb the light energy (UV or visible),

which triggers the formation of reactive species, such as free radicals or cations, which can react with the prepolymer molecules.

Once the reactive species are formed, they react with the monomers/oligomers, causing them to link together through covalent bonds; the polymer chains grow, resulting in the formation of a three-dimensional network. Polymerization can be categorized into two main types: free radical, which is the most widely employed method, and ionic polymerization, specifically cationic or anionic polymerization. Among these, cationic polymerization is the prevailing form.

For the PI to absorb light, there must be an alignment between an emission line from the light source and an absorption band. In such a scenario, the photo-initiator molecule undergoes a process where an electron is promoted to a higher energy orbital, resulting in its electronic excited state, represented as PI* in Equation (1):

$$PI + light \rightarrow PI^* \qquad \text{Eq. (1)}$$

The lifetime of the PI* is typically brief, usually shorter than 10^{-6} seconds. Within this timeframe, the PI* can undergo different pathways: it can revert to its original state (PI) through decay, accompanied by the emission of light and heat, or it can engage in a chemical reaction that produces a reactive intermediate. This reactive intermediate has the potential to react with another radical R·, initiating the polymerization of the monomer. If needed, a reactive diluent can be added to the formulation to adjust its viscosity, facilitating the application of the formulation onto the substrate.[6]

Photopolymerization offers several advantages over other polymerization methods. It is a rapid process since the reaction occurs upon exposure to light, enabling fast curing or solidification of the material. The absence of volatile organic compounds (VOCs) emissions renders the process an environmentally friendly approach. Furthermore, it allows for precise

control over the polymerization process by adjusting the light intensity, exposure time, and formulation. This enables the production of materials with tailored properties.[4,7]

Photopolymerization is widely used in areas such as coatings, adhesives, electronics, and dental materials. The ability to selectively polymerize specific regions using light also finds applications in photolithography, 3D printing, and microfabrication techniques.[8,9]

1.2 Thiol-ene photo-polymerization

In recent years, thiol-ene systems have attracted attention among various classes of UV-curing resins due to their numerous advantages such as: near-zero oxygen or water inhibition during curing, the formation of homogeneous networks, high monomer conversions, reduced shrinkage and residual internal stress, consistent mechanical properties throughout the material, and the relatively low viscosity of the mixture, which minimizes the requirement for a diluent.[5,10,11]

The reactions involving thiols and reactive carbon-carbon double bonds, also known as "enes," possess the features that meet the criteria for modular click reactions or click-chemistry.[11] The thiol-ene reaction is a type of free-radical chain reaction wherein a thiol molecule reacts with an ene group. In an ideal scenario, the predominant mechanism involved is a step-growth mechanism, characterized by a free-radical addition process without any subsequent chain-transfer reaction. This means that homopolymerization does not occur. Moreover, the absence of homopolymerization helps maintain a controlled and uniform three-dimensional network of cross-linked polymer chains. The ability to control the network structure and the degree of cross-linking makes this reaction an attractive choice for various applications, such as in the development of adhesives, coatings, and biomedical materials. Furthermore, the step-growth mechanism ensures that the thiol and ene functionalities are maximally

utilized, resulting in conversions that approach 100%.[4,11] The mechanism is illustrated in Figure 2.

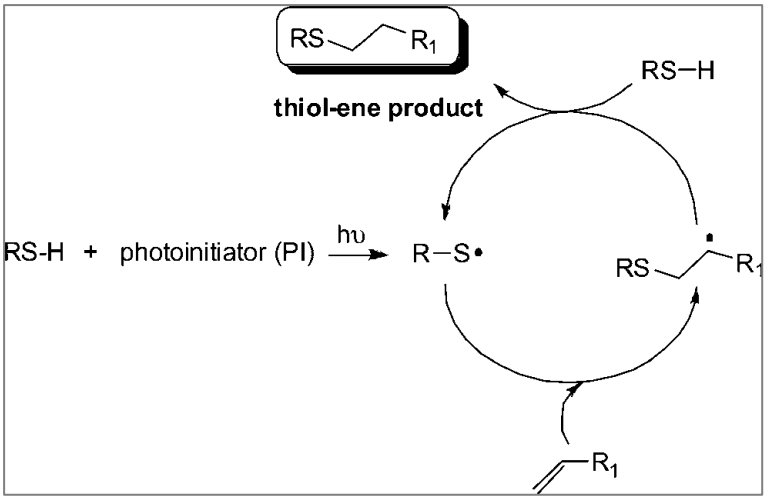

Figure 2: The mechanism of the click-chemistry reaction in presence of a photo-initiator.[13]

Systems like binary thiol–acrylate or ternary thiol–ene–acrylate progresses through three steps reaction: initiation, propagation, and termination. Initiation occurs through the activation of the thiol using the photo-initiator that is exposed to a light source which generates radicals capable of attacking the thiol. The thiol radical then adds to the C=C bond, forming an intermediate radical. In the second step, a chain transfer occurs to a second thiol molecule, resulting in the formation of the polymer chain. Termination events may occur through conventional radical-radical coupling processes.[4,11,12]

Chapter 2

Materials and methods

Lignocellulosic biomass primarily consists of three polymers: cellulose, hemicellulose, and lignin, along with minor components such as acetyl groups, minerals, and phenolic substituents. Depending on the specific type of lignocellulosic biomass, these polymers exhibit varying degrees of organization into complex, non-uniform, three-dimensional structures.

Hemicellulose, the second most abundant polymer, differs from cellulose in its random and amorphous structure. Upon depolymerization, it gives as a result, the formation of several heteropolymers including xylan, galactomannan, glucuronoxylan, arabinoxylan, glucomannan, and xyloglucan. These heteropolymers consist of different 5- and 6-carbon monosaccharide units such as pentoses, C5, (xylose, arabinose) and hexoses, C6, (mannose, glucose, galactose), as well as acetylated sugars.

These C5 and C6 monosaccharides include various compounds such as 1,4-diacids (succinic acid, fumaric acid, malic acid), 2,5-furan dicarboxylic acid (2,5-FDCA), 3-hydroxy propionic acid (3-HPA), aspartic acid, glucaric acid, glutamic acid, itaconic acid, levulinic acid, 3-hydroxybutyrolactone (3-HBL), glycerol, sorbitol, and xylitol/arabinitol.[1] Figure 3 illustrates a diagram presenting the compounds obtained from C5 and C6 monosaccharides.

Furan-based monomers, specifically, have attracted significant interest because of their unique aromatic structure. Two notable molecules for the production of biochemicals and various monomers are 5-hydroxymethyl furfural and furfural. Hydroxymethyl furfural can be derived from C6 sugar units and polysaccharides, while furfural can be obtained by starting with polysaccharides containing C5 glycosidic units.[13]

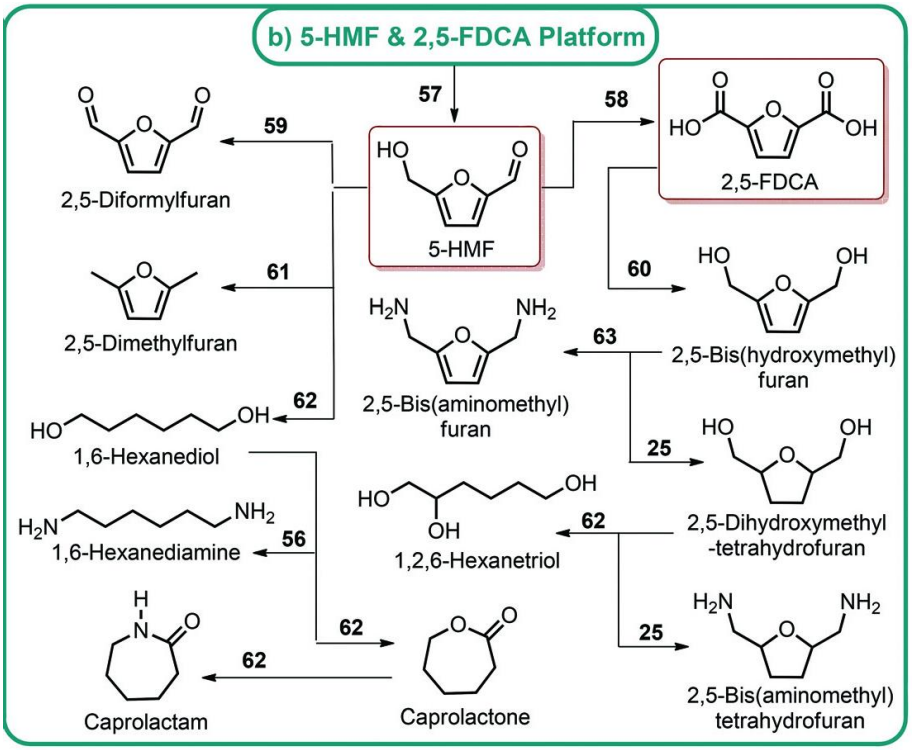

Figure 3: 5-HMF and 2,5-FDCA "platform" chemicals obtained from C5 and C6 monosaccarides.[1]

In this specific study, 2,5-Furandimethanol (FDM) and cis–cyclobutene-1,2-dicarboxylic acids (CBDA-2), were used to synthesize two different furan-based allylated monomers: 2,5-bis((allyloxy)methyl) furan (BAMF) and bisallyl cyclobutane dicarboxylate (BACBDA). These monomers were subsequently employed in a thiol-ene system, UV-cured, and subjected to characterization.

2.1 Synthesis

The monomers, both synthesized and purchased, were utilized without any additional processing. Lorenzo Pezzana, a PhD student, conducted the synthesis of the bi-allylated monomers. The PI, as well as the tri- and tetra-thiols, were purchased from Sigma-Aldrich.

2.1.1 BAMF (2,5-bis((allyloxy)methyl) furan)

The 2,5-Furandimethanol based monomer was synthesised as fallows: FDM (3.00 g) was dissolved in 150 mL of acetonitrile. Then, 3.75 g of pulverized NaOH was added to the mixture and stirred for 30 minutes. Subsequently, 8.1 mmol of allyl bromide (7.02 mL) was slowly added at 0°C. After 3 days at room temperature, the precipitate was filtered and rinsed with acetonitrile. The solvent was evaporated, and extraction was carried out using diethyl ether. The aqueous layer was extracted, and the collected organic phases were washed with water and dried using MgSO4. The solvent was removed under vacuum, yielding 3.96 g of the product (81% yield). Figure 4 illustrates the chemical reaction involved in the process.[3]

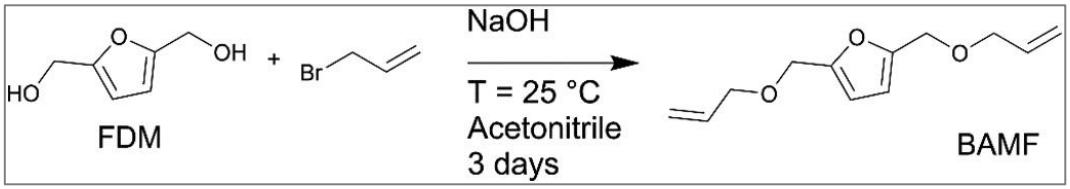

Figure 4: The process of allylation of furfuryl alcohol with allyl bromide.[3]

2.1.2 BACBDA (bisallyl cyclobutane dicarboxylate)

The presence of the unique aliphatic ring in CBDA imparts the final material with noteworthy characteristics such as high tensile strength and a high glass transition temperature. Consequently, CBDA can serve as a green cross-linker in the production of fully biobased thermosets, exhibiting properties comparable to thermosets derived from fossil resources.[3]

Cis- and trans- forms of bisallyl cyclobutane dicarboxylate exist, namely CBDA-1 (trans-cyclobutane-1,3-dicarboxylic acid) and CBDA-2 (cis-cyclobutane-1,2-dicarboxylic acid). For the purpose of this work, the cis-form CBDA-2 is utilized, and henceforth, we will refer to it simply as CBDA.

The synthesis process of bisallyl cyclobutane dicarboxylate based monomer consists of two steps. In the first step, 25 g of Furylacrylic acid was suspended in 250 mL of hexane in a 1000 mL flask. Strong mixing was applied, and UV irradiation was provided using two commercially available lights at 30 W intensity and emission wavelength 385-400 nm. The reaction was monitored by H-NMR analysis. The resulting solid product was filtered through a G4 filter and dried overnight to remove residual hexane. The final product, CBDA, was obtained as a brownish solid (24 g, 97% yield).

The second step involved dissolving 7.00 g of CBDA in 100 mL of dimethyl sulfoxide (DMSO). Then, pulverized NaOH (4.06 g) was added to the solution. Finally, 8.78 mL of allyl bromide was added, and the reaction mixture was maintained at 50°C for 3 days. The reaction was then cooled down to stop further reactions. The organic product was extracted using dichloromethane (DCM), followed by three extractions with water to remove impurities and residual DMSO. The collected organic phase was washed with water and brine, and subsequently dried using MgSO4. The solvent was evaporated under reduced pressure, resulting in a viscous brown liquid as the final product (8.5 g, 94% yield). The process can be seen in Figure 5.[3]

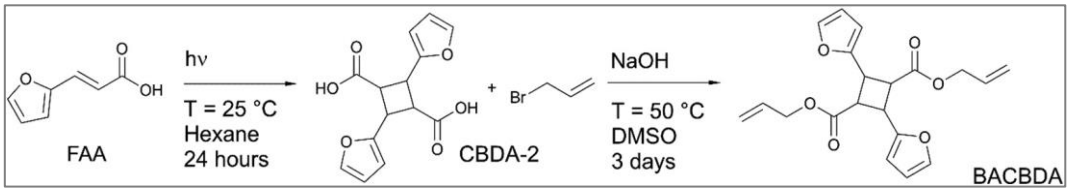

Figure 5: The two steps protocol for the synthesis of BACBDA starting from FAA (trans-3-(2-furyl) acrylic acid).[3]

2.2 Formulation

Four main formulations were investigated. The allyl synthesized monomers (BAMF and BACBDA) were mixed with two commercially available thiols, a tri- and tetra-functional one: trimethylolpropane-tris(3-mercaptopropionate) (TRIS) and pentaerythritol-tetrakis(3-mercaptopropionate) (TETRA). All quantities were considered in moles of functional groups. Figure 6 displays a photograph of the compounds used for the formulations. The thiol-ene formulations were made at fixed stoichiometric ratio of 1:1 between allyl and thiol of functional groups.

Then the photo initiator, Irgacure 819 (BAPO), was added from 1 to 3 phr (parts per hundred) of the entire formulation. To fully dissolve the photo-initiator, the formulations underwent sonication at room temperature for 30 minutes. Shielded vials were used when reagents were mixed to avoid exposure to light.

Figure 6: Compounds used for the formulations.

2.3 Kinetics

2.3.1 Fourier Transform Infrared Spectroscopy (FTIR)

The underlying principle, of the FT-IR, involves directing infrared radiation onto a sample, where it interacts with chemical bonds, leading to the absorption of the incident radiation.[4] When radiation cross a molecule, some specific frequencies will be absorbed if they correspond to the transition of vibrational levels of the molecule.

It can be used to assess substances (solids, liquids, gases, powders, polymers, organics, etc.) that absorb in the mid-infrared (mid-IR), spanning from 4000 cm^{-1} to 400 cm^{-1} (2,5 – 25 µm). Absorption occurs at intrinsic energy levels, specific for each molecule, including organic groups such as carbonyl stretching, alcohol vibration, and C=C double bond vibrations.[14,15]

The system selectively absorbs energy at specific wavelengths, corresponding to defined energies. Fundamentally, transmission-FTIR spectroscopy adheres to the Lambert–Beer law, which implies that there is a linear correlation between the concentration of a compound and its absorbance, given a fixed optical path length. Consequently, FTIR can be used as qualitative and quantitative analysis. However, it cannot detect noble gases, as their vibration does not create a dipole moment, thus do not have absorbance bands in the infrared region of the electromagnetic spectrum.[4,14]

A typical Fourier-Transform Infrared spectrometer consists of a radiation source, a collimating mirror, an interferometer, a sample holder, a detector, an amplifier, an analog-to-digital converter (A/D converter), and a computer. A scheme of a typical FTIR spectroscopy system can be seen in the Figure 7.[14]

For the mid-infrared (mid-IR) region, a common radiation source is a heated silicon carbide, which emits radiation as a black body when heated to approximately 1200 °C.

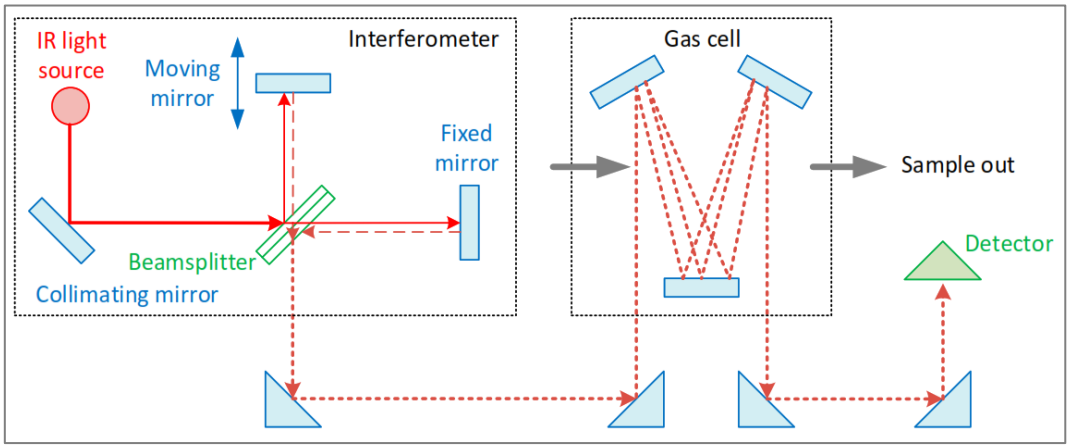

Figure 7: Scheme of a typical FTIR spectroscopy system.[16]

The collimating mirror collects light from the source and makes its rays parallel. The emitted radiation passes through the interferometer, interacts with the sample, and generates a corresponding signal. The interferometer is the central component of an FTIR spectrometer. It consists of a beam splitter, a compensating plate, and a pair of mirrors. Polychromatic infrared light emitted by the source is collimated towards the beam splitter usually in KBr. Ideally, 50% of the light is directed towards the fixed mirror, while the other 50% is directed towards the moving mirror. The difference in optical path length between the two paths creates constructive and destructive interference, resulting in a well-defined wavelength single light beam reaching the sample. This light beam interacts with the sample and then reaches the detector.[14,15]

The scanning of the interferometer generates an interferogram, which plots the signal intensity against the optical path difference. The spectrum is obtained through Fourier transformation of the interferogram.[4]

There is a different setup, which addresses certain issues associated with traditional FTIR such as sample preparation and reproducibility, called

ATR-FTIR (Attenuated Total Reflection Fourier Transform IR Spectroscopy). In this setup, the sample is placed on a crystal (e.g. KBr, C) with a high refractive index. The infrared beam interacts with the sample at the surface, approximately for 0.5 µm to 5 µm, before being reflected back towards the crystal, which then redirects the beam towards the detector. The detector measures the wave changes induced by the sample's interaction with the crystal. This setup allows for the analysis of both solid and liquid materials, providing qualitative and quantitative information.[4]

One notable advantage of FTIR is the ability to monitor reactions in real-time, observing shifts and changes in peaks that correspond to modifications in chemical bonds occurring during the reaction. This is known as real-time FTIR (RT-FTIR). The technique can be applied at different temperatures by heating the crystal, and it can also track photochemical reactions.

In this study a Thermo Scientific Nicolet iS 50 Spectrometer was used, in transmission mode to monitor the photo-curing process. Then the Omnic Thermo Fischer Scientific Software was used to handle the spectra afterwards.

A liquid formulation film, approximately 32 µm thick, was applied onto a SiC (silicon carbide) window, then the film was subjected to scanning under a nitrogen atmosphere. Following the scanning, the film was exposed to UV irradiation with increments of 5 seconds using a DYMAX ECE 5000 Flood halide lamp from Dymax Europe GmbH, and a spectrum was obtained. The UV-light source utilized had an intensity of around 130 mW/cm^2, centred at 365 nm.

The spectra acquired were between 400 and 4000 cm^{-1} after 32 scans with and a resolution of 4 cm^{-1}. The disappearance of carbon-carbon peaks at 810 cm^{-1}, 1630 cm^{-1} and the thiol (S-H) group at 2250 cm^{-1} were monitored to calculate the conversion with the following relations:

$$Conversion\ (\%) = \left(\frac{\left(\frac{A_1}{A_{ref}}\right)_{t=0} - \left(\frac{A_1}{A_{ref}}\right)_t}{\left(\frac{A_1}{A_{ref}}\right)_{t=0}} \right) \times 100 \qquad Eq.1$$

$$Conversion\ (\%) = \left(1 - \frac{A_1}{A_{t=0}}\right) \times 100 \qquad Eq.2$$

where A_{ref} is the peak taken as reference at 1720 cm^{-1}, that doesn't change with the proceeding of the crosslinking reaction. The A1 is the peak under investigation: 810 cm^{-1}, 1630 cm^{-1} and 2250 cm^{-1}. Eq. 2 was used for more noisy spectra.

2.3.2 Photo – Dynamic Scanning Calorimetry (Photo – DSC)

Differential scanning calorimetry (DSC) is an effective analytical tool for characterizing the physical properties of a polymer. Is a technique that provides both qualitative and quantitative information about the thermal properties of solid materials.

The energy-related properties, specifically heat capacity (Cp) and its integral over temperature (enthalpy, H), obtained through calorimetric measurements, possess a well-defined physical significance. It can determine phase transformations such as melting, glass transition temperature (Tg), degradation temperatures, crystallization, polymorphisms and parameters as specific and latent heats, enthalpy, and material purity.

Phase transformation refers to the change of matter from one state to another, such as solid to liquid or liquid to gas. This transformation is driven by the chemical potential, which is influenced by temperature and pressure. When there is a gradient in chemical potential between two phases, a spontaneous phase transition occurs from the higher potential phase to the lower potential phase, continuing until equilibrium is reached. In equilibrium, the chemical potential between the phases is zero.

Phase transitions can be categorized as first-order and second-order. First-order transitions involve changes in thermodynamic properties like

entropy, enthalpy, or volume. They are characterized by the absorption or release of latent heat during isothermal changes, such as liquid-solid, solid-liquid, and gas-liquid transitions. Examples of first-order transitions include crystallization, melting, condensation, and evaporation. Second-order transitions, on the other hand, do not involve a change in latent heat or volume. Instead, properties like heat capacity, isothermal compressibility, and the coefficient of thermal expansion are modified. A commonly observed second-order transition in polymers is the glass transition temperature (Tg), which reflects changes in molecular mobility and relaxation time in amorphous solids.

Tg is a time- and temperature-dependent transition between the rubbery and glassy states, but it is considered a state transition rather than a phase transition due to the unbalanced nature of the glassy state and the wide range of temperatures at which vitrification can occur.[16]

The Figure 8 illustrates a representative example of thermal transitions in a semicrystalline material.

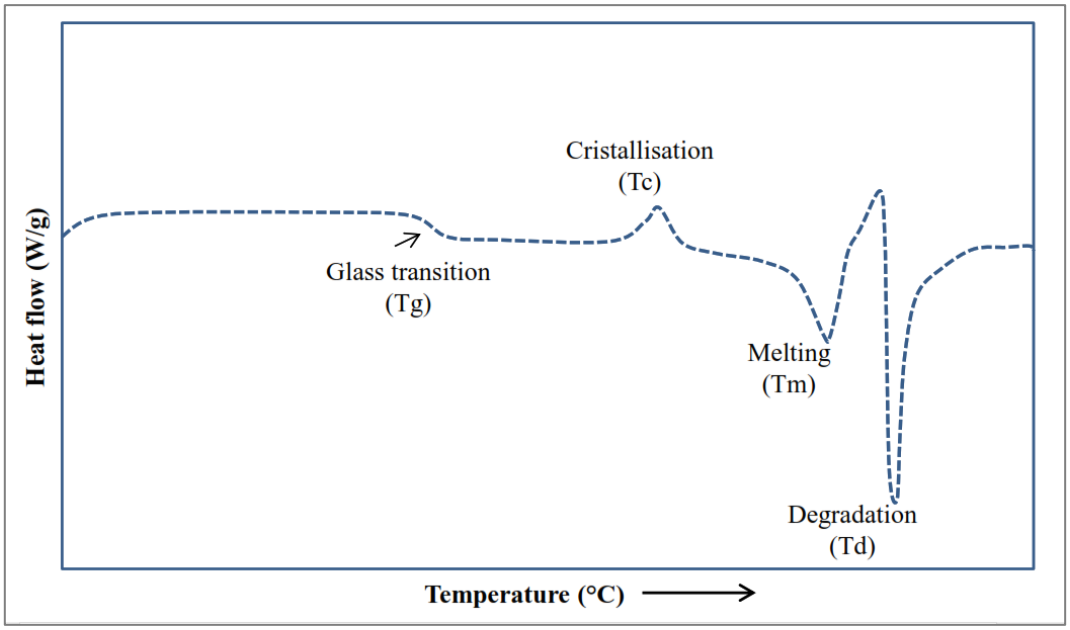

Figure 8: Example of thermal transitions in semicrystalline material.[16]

The test is conducted in a chamber containing two crucibles: one with the sample and the other, usually empty, as reference. The instrument measures the difference in heat flow between the two crucibles as a function of temperature and time giving as output a thermogram. By using identical heating ramps and temperature cycles, the Tg values of different materials can be determined and compared. Additionally, it is possible to select a specific atmosphere for the analysis, depending on the requirements of the study such as air, nitrogen, or oxygen.

A configuration known as Photo-DSC was utilized to investigate the photo-curing process by coupling the DSC instrument with a radiation source (UV/Visible) during the analysis. By integrating the radiation source with the DSC, it becomes possible to monitor the thermal behaviour of the sample while simultaneously exposing it to the UV/Visible radiation. This unique combination allows for the in-situ study of the crosslinked network formation.

In this study, the investigation was carried out by using a Mettler TOLEDO DSC-1 with a Gas Controller GC100 equipped with a mercury lamp, Hamamatsu LIGHTINGCURE LC8. An optical fiber was used to directly irradiate with UV light the sample pan (40 µL), while an empty pan served as a reference. The UV-source was centred at 365 nm with an intensity of approximately 100 mW/cm^2.

The analysis was conducted at RT in a nitrogen atmosphere with a flow of 40 mL/min. Figure 9 illustrates a diagram of the instrument used for the analysis.[17]

The samples were irradiated for two cycles, the second cycle was performed to confirm complete curing and establish a baseline; then the second curve was subtracted from the first. The energy resulting from the various samples, as the integration of the curve, were then compared to the pristine reagents. The time at which the peak occurs gives an estimation of the reactivity of the system.

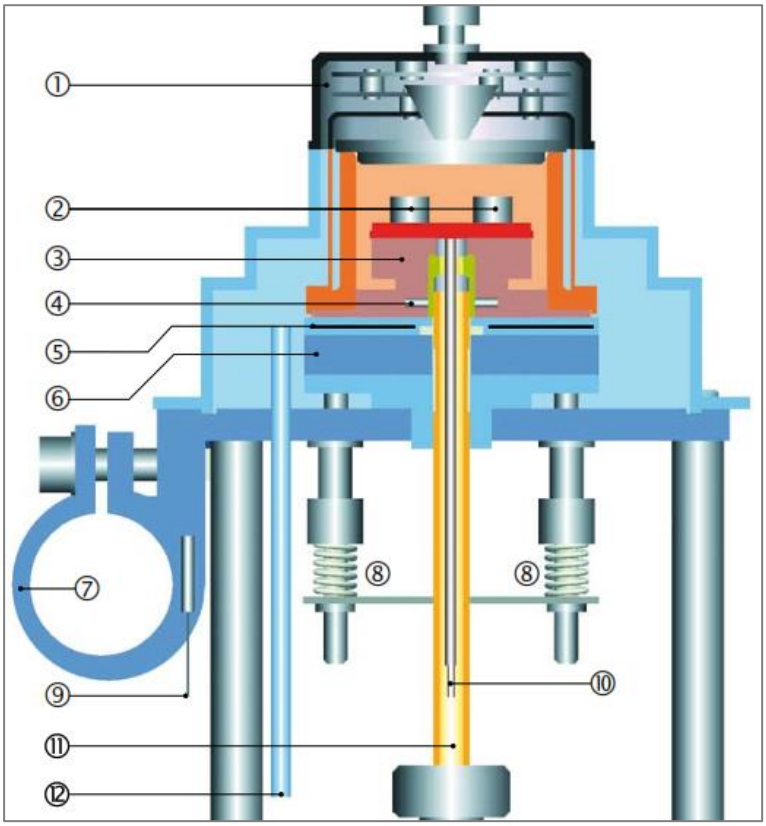

Figure 9: General scheme of DSC apparatus.[17]

1. Furnace lid
2. Crucibles on the DSC sensor
3. Silver furnace
4. PT100 of furnace
5. Flat heater between two insulating disks
6. Thermal resistance for cooler
7. Cooling flange
8. Compression spring construction
9. Cooling flange PT100
10. DSC raw signal for amplifier
11. Dry gas inlet
12. Purge gas inlet

2.3.3 Photo – rheology

This approach combines rheology analysis with the use of UV/visible radiation to monitor the dynamic changes in mechanical properties as the cross-linking reaction takes place. It is a valuable method for studying reaction kinetics.

To perform this technique, the liquid formulation is placed onto a quartz substrate, and after a period of stabilization, a UV source is activated, directed towards the sample, initiating the reaction. By examining parameters such as curve slopes, induction time, and reaction velocity, meaningful comparisons can be made between different formulations. A higher slope indicates increased reactivity, while the absence of an induction time suggests an immediate start of the reaction. These parameters are helpful in determining the optimal conditions for the duration of irradiation to achieve the desired properties.

The curing process was investigated using photo-rheology, which involved using an Anton Paar MC 302 rheometer equipped with a plate-plate geometry. A metal disk with an outside diameter of 25mm and a quartz disk were used as the top and bottom plates, respectively, with a distance of 150µm between them.

Liquid sample, around 150 µL, was placed between the plates, and the UV light was directed onto the sample using an optic fiber after 60 seconds of stabilization. A Hamamatsu LIGHTINGCURE LC8 was used as the UV-visible light source, providing a light intensity of approximately 40 mW/cm^2 on the surface of the sample. The measurements were performed under oscillatory conditions at a frequency of 1 Hz with a strain of 1% at room temperature. The Figure 10 depicts the setup for the photo-rheology used in this study.[4]

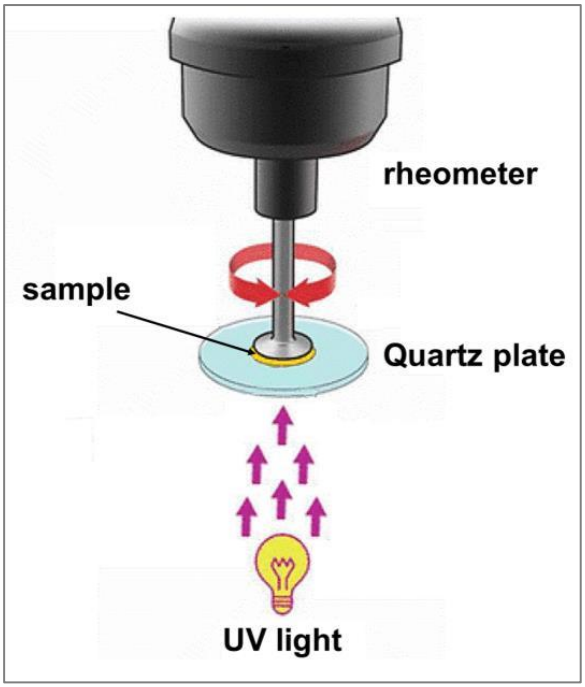

Figure 10: Scheme of a photo-rheology setup.[4]

2.4 Thermo-mechanical characterization

2.4.1 Dynamic Mechanical Thermal Analysis (DMTA)

Dynamic mechanical thermal analysis (DMTA) is a method for determining the glass transition temperature (Tg) and other mechanical proprieties of a polymer. It involves subjecting the sample to a constant oscillatory input, either stress or strain, while increasing the temperature.

When a polymer material is exposed to sinusoidal stress, its response can be divided into two components: elastic behaviour, represented by the storage modulus (E'), and viscous behaviour, represented by the loss modulus (E'').

The ratio of the loss modulus and the storage modulus gives the damping factor, known as the tanδ value. This value indicates the amount of energy dissipated during a cycle of deformation. The Tg of the material is conventionally considered as the peak in the tanδ curve, and it is a crucial

parameter for thermoset polymers as it correlates with the crosslink density. Higher crosslink density corresponds to a higher Tg, which is also associated with higher degree of conversion. An estimation of the cross-linking density was evaluated by the Eq.3:

$$\nu_c = \frac{E^*}{3RT} \qquad Eq.3$$

with E* the storage modulus at the rubbery plateau, around Tg + 50 ◦C, R the gas constant, and T the temperature expressed in Kelvin.[3]

The glass transition temperature is a significant characteristic of a polymers: it signifies the transition from a glassy state (T < Tg), where the material is solid, stiff, and rigid, to a rubbery state (T > Tg), where the material becomes more flexible due to increased segmental mobility.

A Triton Technology instrument was used for the thermo-mechanical analysis, in temperature sweep mode. The temperature ramp was set at a rate of 3 °C/min beginning from RT (or -60 °C when necessary) to 180°C if required. The applied tensile stress frequency was 1Hz and a strain rate of 0.1%. The value of the glass transition was determined by the peak of the tanδ curve.

The examined specimens (0.2 × 3.5 × 12 mm.) were subjected to UV curing in silicon moulds under a DYMAX ECE 5000 Flood halide lamp. The utilized UV light source had an approximate intensity of 130 mW/cm^2 and

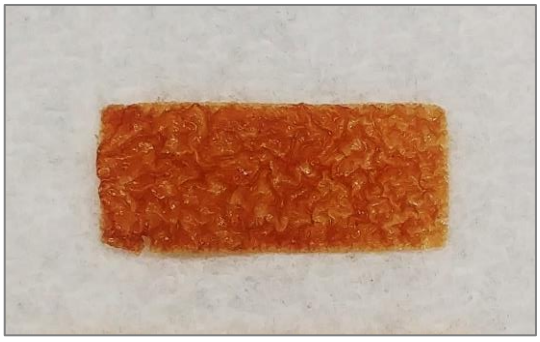

Figure 11: Photo of a BACBDA sample for DMTA tests.

was centred at 365 nm. Figure 11 shows a representative photograph of a BACBDA sample used for DMTA tests.

2.4.2 Tensile

An MTS QTestTM/10 Elite instrument and TestWorks® 4 measurement software from MTS System Corporation were used to conduct a tensile test to analyse the mechanical properties of the samples. The test was performed with a 1000 N load cell and a speed of 5 mm/min on the samples that had a mean size of 0.2 × 5 × 50 mm. The stress-strain curve was recorded, and the Young's modulus (E) was determined by calculating the slope of the linear region of the curve. The reported outcome represents the average value obtained from five measurements.

Furthermore, the samples were made under the same conditions used for the DMTA tests. Figure 12 displays a photograph of a BACBDA sample used for tensile tests as an illustrative example.

Figure 12: Photo of a BACBDA sample for tensile tests.

2.4.3 Contact angle and hardness

To assess the coating properties such as contact angle and hardness, the formulations were subjected to UV-curing on a glass substrate, creating a uniform film with a thickness of 150 μm.

The contact angle evaluation involved conducting tests on the exposed surface using water as the test liquid. For this purpose, a Drop Shape Analyzer, specifically the DSA100 by Krüss, was utilized.

On the other hand, the hardness measurement was carried out using a Sauter HMO mobile Leeb Hardness Tester, following the ASTM A956 standard.

In order to obtain reliable results, five measurements were performed, and their average value was calculated for each property being evaluated.

Chapter 3

Results and discussion

3.1 Kinetics

3.1.1 FTIR

The curing process was investigated firstly by FT-IR analysis. The 930 cm^{-1} and 2570 cm^{-1} peaks were monitored to evaluate the conversion. The peak areas related to C=C (930 cm^{-1}) and S–H (2570 cm^{-1}) bonds decreased as a function of irradiation time indicating the reaction progression of the thiol-ene functional groups. The conversion was calculated using Eq. 1.

As a first step we evaluated the effect of photo-initiator content in the curing process. Specifically, we examined the conversion of C=C and S-H groups by varying the concentration of BAPO from 0 to 3 phr. As a result, it was observed that increasing the amount of BAPO yielded a higher final conversion rate and a slight enhancement in the photopolymerization rate (Figure 13).

While thiol-ene reactions can theoretically occur in the absence of a photo-initiator, our findings demonstrated that the presence of 3 phr of BAPO significantly enhanced reactivity and increased thiol-ene conversion. This outcome can be attributed to the increased generation of radicals by the photo-initiator upon irradiation. With more radicals available, the polymerization kinetics were accelerated, leading to a greater degree of conversion. Consequently, incorporating BAPO in the preparation of UV-

cured coatings proved to be beneficial for achieving improved reactivity and higher conversion rates.

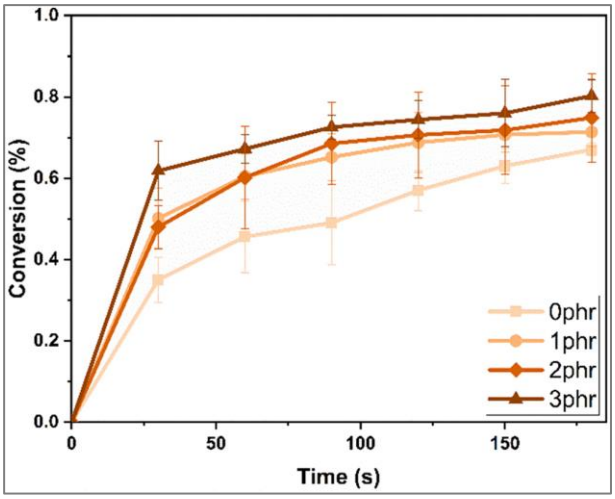

Figure 13: Impact of the photo-initiator, at 0, 1, 2, and 3 phr, on the conversion.

The characteristic click reaction nature of the thiol-ene system was confirmed by comparing the conversion trends of the two functional groups (C=C and S-H), as shown in Figure 14. The conversion of both groups exhibited similar tendencies, indicating a 1:1 ratio between the two functional groups, which is a key feature of thiol-ene click reactions.

Real-time FTIR analysis was performed on all formulations, and the conversion results are presented in Table 1.

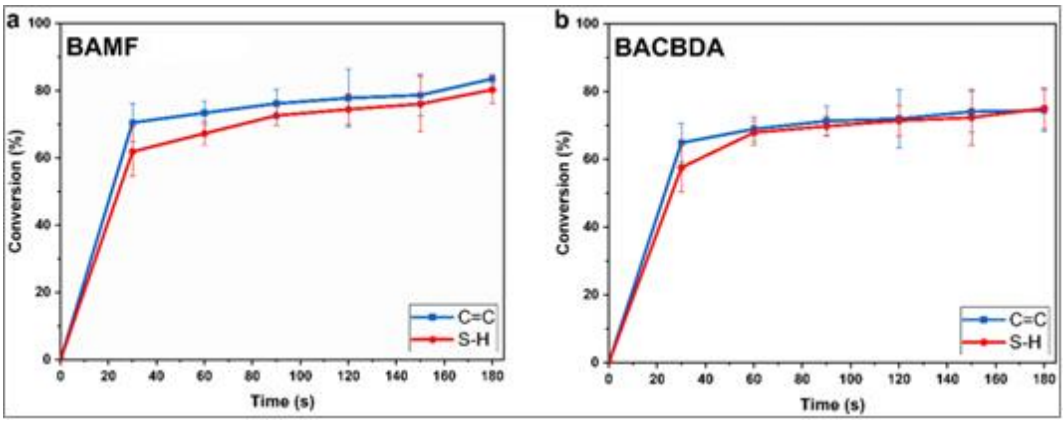

Figure 14: Conversion of the two functional groups monitored (C=C and S-H) for both formulations: BAMF/TRIS on the left and BACBDA/TRIS on the right.

The results show that the final conversion rates were similar across all formulations incorporating both BAMF and BACBDA monomers. However, it is important to note that the BACBDA formulation exhibited a slightly lower conversion value, which can be attributed to the higher steric hindrance of the allyl monomer in comparison to the formulation containing BAMF. Additionally, the UV-Vis results later revealed that BACBDA exhibited higher UV absorption, which could have limited the crosslinking process. Despite this difference, conversion values exceeded 70%, indicating that all the synthesized allyl monomers displayed excellent reactivity to UV light and a cross-linked network was formed. These findings provide evidence of the suitability and effectiveness of the UV-curing process in achieving significant conversion rates for the allyl monomers, thereby reinforcing the potential exploitation of these formulations in practical coating applications.

Table 1: Conversion results for all formulations.

Formulation	S-H conversion (%)	C=C conversion (%)
BAMF/TRIS	80±4	83±1
BAMF/TETRA	75±1	74±1
BACBDA/TRIS	74±2	77±2
BACBDA/TETRA	72±3	65±5

3.1.2 Photo – DSC

The photo-DSC method was used to investigate the heat release during curing and time to peak during network formation. The influence of the photo-initiator amount (from 0 to 3 phr) on the UV curing process was investigated by analysing the curing peak. Figure 15 displays an example of photo-thermogram obtained for BAMF/TRIS formulation. All formulations exhibited a similar trend.

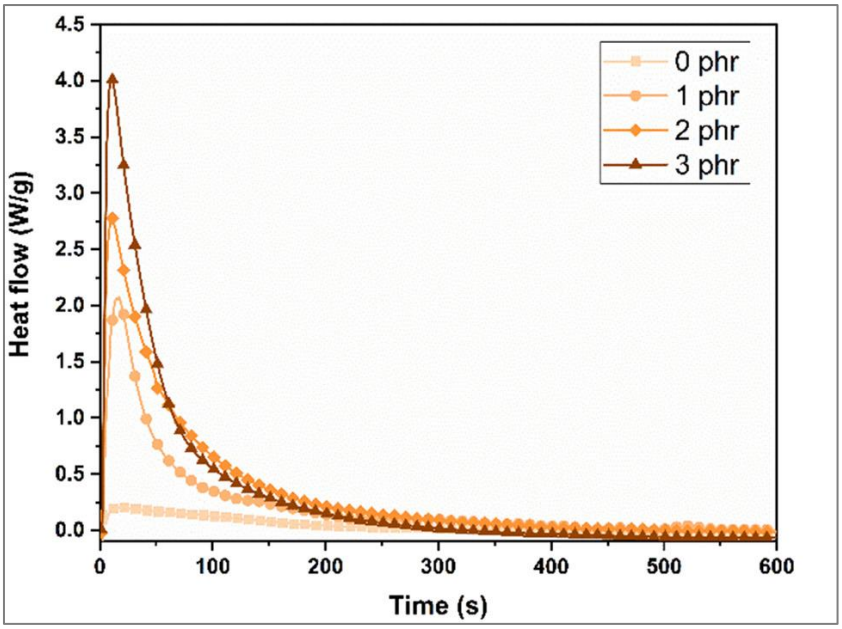

Figure 16: DSC heat release with increasing amount of photo-initiator for BAMF/TRIS formulation.

The increase in ΔH, calculated by the integration of the curve, after the addition of the photo-initiator supports the findings from the real-time FTIR analysis. Additionally, the investigation of h_{peak} (peak height at the maximum of the DSC curve) revealed that the highest value was achieved with 3 phr of the photo-initiator (Figure 16). It is known that h_{peak} is

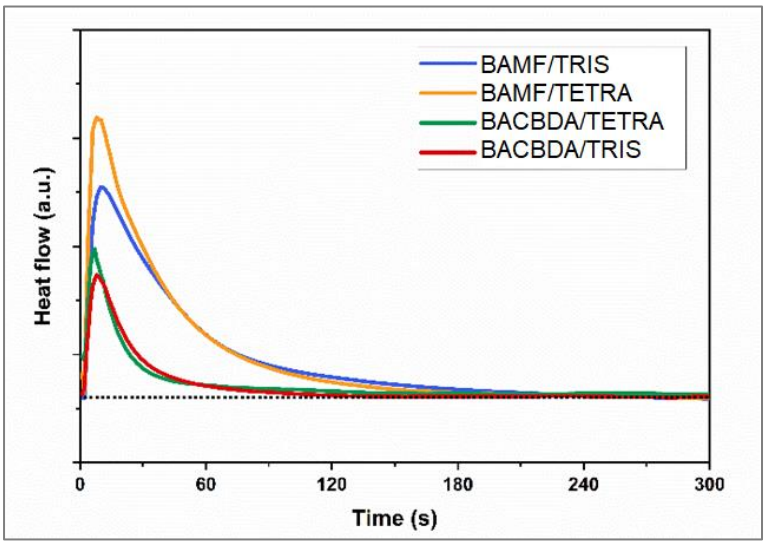

Figure 15: DSC heat release of all formulations with 3 phr of photo-initiator.

proportional to the rate of polymerization, indicating the beneficial effect of the initiator on the reaction kinetics.

Furthermore, the t_{peak} (time to the maximum rate of polymerization) decreased with an increasing amount of the photo-initiator.

It is possible to evaluate the conversion by comparing the theoretical ΔH with that obtained by integrating the thermogram resulting from the experiment. The conversion of all different formulations was evaluated using the following equation:

$$Conversion\ (\%) = \left(\frac{\Delta H_{experimantal}}{\Delta H_{theoretical}}\right) \times 100 \qquad Eq.4$$

Considering 79.5 kJ/mol as the theoretical heat release value for the reaction between an ene and thiol group[18] the conversions were calculated (Table 2).

The photo-DSC analysis exhibited a lower degree of conversion compared to the real-time FTIR data, and this discrepancy can be attributed to the sample configuration. In the real-time FTIR analysis, the sample was evenly spread with a thickness of 32 μm, which led to minimal light absorption by both the monomer and the formed polymer. As a result, the FTIR analysis accurately captured the conversion process without interference from light absorption effects. On the other hand, during the photo-DSC analysis, the sample was contained within the DSC pan, which limited the penetration of light irradiation, especially in the BACBDA-based formulations. This restricted light exposure resulted in a less comprehensive assessment of the conversion process in the DSC analysis. Therefore, the difference in sample thickness and the partial light absorption in the DSC pan are key factors contributing to the lower degree of conversion observed in the photo-DSC analysis when compared to the real-time FTIR data.

Table 2: Photo-DSC results and conversion of C=C double bonds.

Formulation	h_{peak} (W/g)	ΔH_{exp} (J/g)	C=C conversion (%)
BAMF/TRIS	3,9±0,4	210±12	62
BAMF/TETRA	4,5±0,5	225±10	64
BACBDA/TRIS	2,5±0,4	90±13	35
BACBDA/TETRA	3,1±0,8	75±15	28

In order to examine the potential absorption characteristics of the ene-monomers, a UV-Vis analysis was carried out to assess their light absorption behaviour. The obtained results are presented in Figure 17.

Both monomers displayed absorption peaks attributed to the presence of the furan ring in their chemical structure. However, it was observed that BACBDA exhibited a significantly higher absorption region compared to BAMF monomer. This heightened absorption capacity of BACBDA might lead to an interference with UV light during the bulk polymerization process, potentially limiting the overall conversion, as observed in FT-IR analysis.

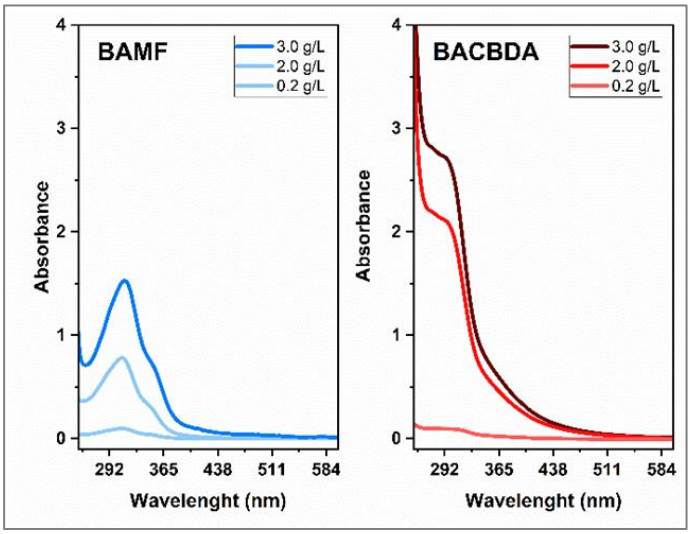

Figure 17: UV-vis absorption spectra of furan-based ene monomers. BAMF on the left and BACBDA on the right.

The increased light absorption of BACBDA could result in reduced availability of UV photons for initiating the photopolymerization reaction, thereby affecting the efficiency of the curing process. This finding emphasizes the importance of considering the specific light absorption characteristics of ene-monomers in UV-curing systems and highlights the potential influence of monomer absorption on the overall photochemical reaction kinetics.

To confirm the feasibility of cross-linking bulk samples for mechanical characterization, gel percentage measurements were performed on the UV-cured samples to assess the fraction of gel present after irradiation. The summarized results can be found in Table 3. The BAMF/TRIS thermoset exhibited the highest value of gel content. Similarly, the BAMF/TETRA-based thermoset also showed a considerable gel content, although slightly lower than the BAMF/TRIS thermoset. On the other hand, the gel content decreased in the case of BACBDA-based formulations, suggesting a less effective cross-linking process.

The lower gel content for the thermoset containing BACBDA monomer confirmed the DSC results and highlighted the limitations in polymerization due to steric hindrance and light penetration. However, the gel percentage values demonstrated the effective formation of an insoluble fraction resulting from cross-links between polymer chains, confirming the potential for coating development.

Table 3: Gel content of all formulations.

Formulation	Gel content (%)
BAMF/TRIS	80±2
BAMF/TETRA	78±3
BACBDA/TRIS	72±4
BACBDA/TETRA	68±3

3.1.3 Photo – rheology

To gain a more comprehensive understanding of the photocuring process, real-time photo-rheology experiments were conducted. In this approach, the evolution of the curing process was analysed by monitoring the trend in viscosity and storage modulus. During UV exposure, the viscosity of the resin increased, causing a rise in the storage modulus, which eventually reached a plateau once the reaction was completed.

Figure 18 presents the results obtained for the formulations based on BAMF and BACBDA. The variation in the curves is attributed to the initial induction time of the reaction. The formulations containing BACBDA exhibited a longer induction time, as the increase in storage modulus was delayed compared to the formulation containing BAMF. Moreover, both formulations required more time to reach the plateau of the storage modulus. The curves of the FDM-based network achieved a constant modulus value after approximately 360 seconds, while the formulation containing the CBDA-based monomer took 900 seconds.

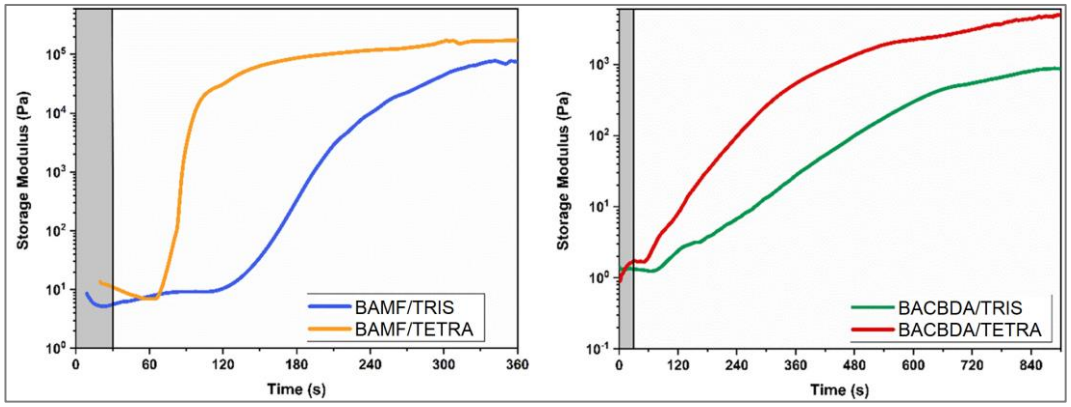

Figure 18: Photo-rheology of all formulations. On the left the BAMF-based formulations and on the right the BACBDA-based formulations.

This distinct behaviour, which is in agreement with FT-IR and photo-DSC analysis, can be explained by the light absorption characteristics of the ene monomers. When UV light is directed onto the sample, two processes can occur. The first involves the absorption of light by the photo-initiator,

generating radicals that initiate the crosslinking reaction. The second process entails direct absorption of light by specific chromophore groups present in the monomer's structure, which does not lead to radical generation. In the case of allyl derivatives, it is crucial to consider the UV-vis spectra obtained (Figure 17). The radiation absorption by the monomers can interfere with the UV emitted by the lamp, reducing the available dose for the formation of radical species. As a result, formulations containing BACBDA required a longer induction time to accumulate the necessary radiation dose for initiating the curing reaction.

Overall, real-time photo-rheology provided valuable insights into the curing kinetics of the formulations, highlighting the impact of monomer absorption characteristics on the initiation and progression of the photocuring process. These findings underscore the significance of considering specific monomer properties and light absorption behaviour when designing efficient UV-cured materials.

3.2 Thermo-mechanical characterization

3.2.1 DMTA

The thermomechanical properties of the UV-cured thiol-ene networks were investigated using the DMTA technique. Figure 19 presents the tan δ and storage modulus curves as a function of temperature for all the formulations studied in this work. The main objective was to tailor the thermomechanical characteristics of the UV-cured coatings by modifying the thiol functionalities and ene structures.

The impact of different thiols in BAMF-based formulations was first examined. As illustrated in Figure 19, the UV-cured BAMF/TETRA resin displayed a higher glass transition temperature (Tg) of -13 °C compared to BAMF/TRIS (-26 °C). This result can be explained by the thiol-monomer functionalities. The increased number of thiol groups contributed to a higher

rigidity and a higher Tg of the final coating; this trend is in accordance with other work found in literature.[19–21] A higher crosslinking density derives from a greater number of thiol functionalities. The observed high gel content further supports the presence of a high crosslinking density.

Next, the impact of bis allyl structures was investigated by comparing the TRIS-based formulations. A remarkable 38 °C increase in Tg was observed when BACBDA was used instead of BAMF, which can be attributed to the inherent rigidity of CBDA-2 derivatives possessing a rigid cyclobutane ring which imparts greater structural stability, resulting in improved thermo-mechanical properties. A similar effect was observed in the BACBDA/TETRA thermoset, where the chemical structure of the allyl monomer led to an approximately 35 °C higher Tg compared to the BAMF/TETRA moiety. Furthermore, BACBDA/TETRA exhibited a

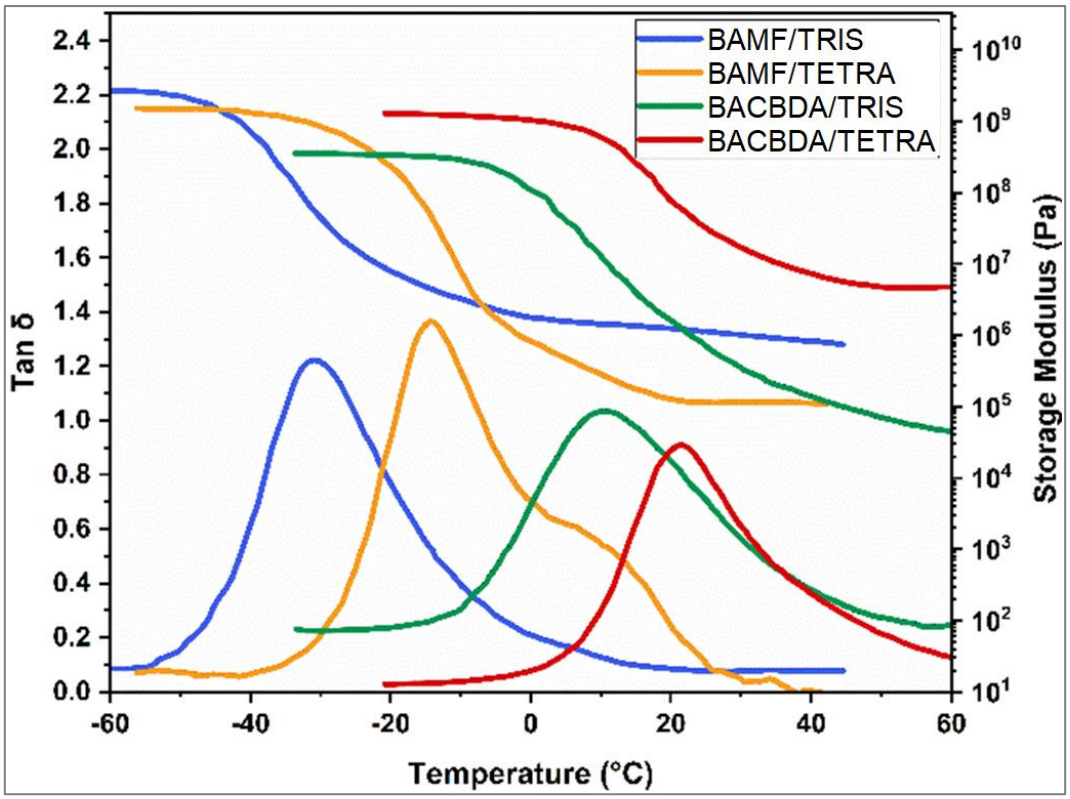

Figure 19: DMTA curves (tan δ and Storage modulus) for all formulations.

higher Tg (24 °C) compared to other biobased thiol-ene thermosets derived from ferulic acid, isosorbide, and eugenol.

The evaluation of cross-link density revealed an increase from BAMF/TETRA to BACBDA/TETRA, following the same trend as Tg. Despite the lower conversion, BACBDA/TETRA demonstrated the highest Tg and cross-link density. This underscores the potential for achieving excellent performance by leveraging the rigid chemical structure and high monomer functionality of CBDA-2.

BAMF/TRIS exhibited a cross-link density value of 149 mmol/dm3, comparable to BACBDA/TRIS, despite having a lower Tg. This can be explained by the higher conversion level and increased gel content achieved in the formulation containing BAMF/TRIS. As discussed earlier, this particular formulation exceeded 80% conversion, resulting in a high cross-link density.

These findings highlight the significance of selecting appropriate monomers and understanding their unique structural characteristics for tailoring the thermomechanical properties of UV-cured coatings. In Table 4 we summarized the results.

Table 4: Thermo-mechanical proprieties evaluated by DMTA and DSC.

Formulation	DMTA Tg (°C)	DSC Tg (°C)	E' ($\times 10^6$ Pa)	ν_c ($\frac{mmol}{dm^3}$)
BAMF/TRIS	-26±4	-14±8	1,10	149
BAMF/TETRA	-13±4	-3±7	0,14	18
BACBDA/TRIS	12±3	8±5	0,50	61
BACBDA/TETRA	24±3	19±4	4,25	490

3.2.2 DSC

DSC analysis was conducted to validate the findings obtained from DMTA. The four different formulations were UV-cured under identical conditions. The observed trend in the DMTA results was confirmed by the DSC measurements as shown in Table 4. The Tg data evaluated by DSC analysis are collected in Table 4 as well.

3.2.3 Tensile

Tensile tests were performed on the UV-cured coatings to assess their mechanical properties. The thermosets exhibited elastic behavior with noticeable strain at break, which can be attributed to their relatively low Tg values, as reported in Table 4. All the tested samples were within the rubbery region, above the Tg, at room temperature.

Figure 20 illustrates the typical stress-strain curves obtained for the thiol-ene UV-cured networks and Table 5 summarizes the results with $\sigma 0$ ($sigma_0$) being the stress at break and ϵ_0 the strain at break.

A consistent trend emerged when comparing formulations using TETRA and TRIS with the synthesized monomers. The higher number of thiol functionalities in TETRA led to higher elastic modulus and stress at break. This result aligns with the higher Tg values reported previously. Particularly, BACBDA/TETRA exhibited the highest stress at break and elastic modulus. The tensile properties corroborated and supported the findings obtained from DMTA analysis, providing additional evidence for the improved mechanical characteristics achieved by utilizing BACBDA/TETRA formulation.

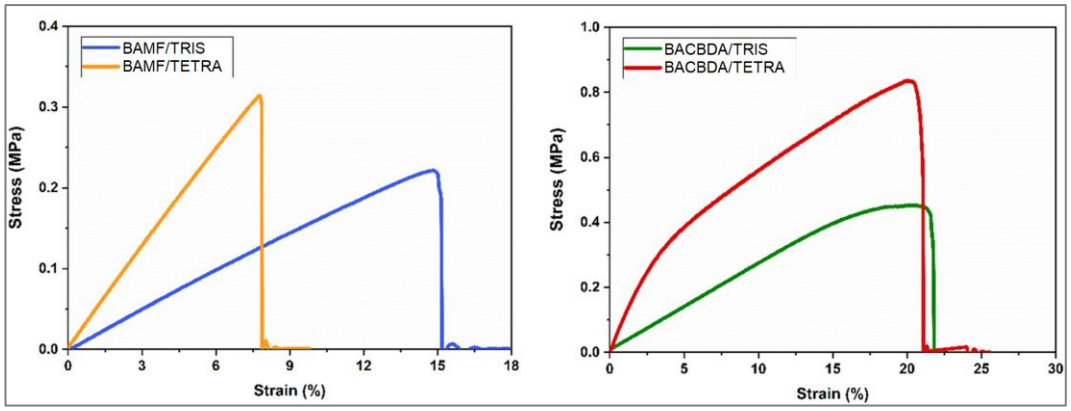

Figure 20: Stress-strain curves. BAMF-based samples on the left and BACBDA-based samples on the right.

The toughness of the coatings was evaluated by calculating the area under the stress-strain curve. The trend revealed the highest value for BACBDA/TETRA at 11.44×10^4 J/m^3. The use of BACBDA resulted in increased toughness compared to the coating containing BAMF. As mentioned before, the higher rigidity of the structure derived from the cyclobutane ring could contribute to this property, along with the higher cross-link density achieved.

Overall, the tensile test results demonstrate the successful tailoring of the mechanical properties of UV-cured coatings by thoughtfully selecting different thiol-ene monomers. The higher number of thiol functionalities and the specific chemical structure of the BACBDA monomer contribute to its superior performance in terms of elastic modulus, stress at break, and toughness, making it a promising candidate for high-performance coatings applications.

Table 5: Tensile tests results.

Formulation	E (MPa)	sigma$_0$ (MPa)	ϵ_0 (%)	Toughness (×10^6 J/m^3)
BAMF/TRIS	1,7±0,3	0,21±0,02	14,5±0,6	1,33±2,7
BAMF/TETRA	4,1±0,4	0,33±0,06	8,5±1,3	1,78±5,0
BACBDA/TRIS	2,2±0,3	0,37±0,07	20,5±0,8	4,83±5,6
BACBDA/TETRA	9,7±1,3	0,93±0,13	20,8±1,3	11,44±3,23

3.2.4 Coating properties

Contact angle measurements were conducted to evaluate the wettability of the sample surfaces. Notable differences in surface hydrophobicity were observed when transitioning from tri- to tetra-thiol, as well as when changing the bis-allyl monomers. This change in hydrophobicity can be attributed to both the differences in chemical structure and the conversion of thiol groups.

The transition from TRIS to TETRA led to an increase in surface hydrophobicity, likely due to the presence of more thiol functional groups, which enhances cross-linking density and surface rigidity. Similarly, the use of BACBDA instead of BAMF also resulted in increased hydrophobicity. The rigid cyclobutane ring in BACBDA imparts higher surface hydrophobicity compared to the furan ring in BAMF.

Regarding hardness, the presence of the tetrafunctional thiol, led to higher values compared to the samples containing TRIS, as well as the BACBDA-based formulations compared to the BAMF-based ones. The enhanced hardness can be attributed to the higher Tg values achieved in the TETRA-based formulations, indicating a greater degree of cross-linking and increased rigidity. The higher number of thiol functionalities in TETRA promotes more efficient cross-linking, resulting in a harder and more rigid surface. The key results are presented in Table 6.

Table 6: Contact angle and hardness.

Formulation	Contact angle (°)	Hardness (HL)
BAMF/TRIS	62±4	156±12
BAMF/TETRA	66±3	245±29
BACBDA/TRIS	72±2	195±23
BACBDA/TETRA	74±4	296±33

Overall, the assessment of surface properties provides valuable insights into the influence of thiol functionalities and bis-allyl monomers on the surface characteristics of the UV-cured coatings. The combination of chemical structure, thiol functionality, and conversion levels plays a crucial

role in determining the hydrophobicity and hardness of the coatings. The comprehensive understanding of these surface properties is essential for tailoring coatings for specific applications that require specific wettability and mechanical properties.

Chapter 4

Conclusions

By synthesizing biobased allyl derivatives, the aim of this work is to explore environmentally friendly and sustainable alternatives to commercial fossil-based monomers in UV-Curing process. The current research focuses on the UV-induced cross-linking of furan-based allyl monomers using thiol-ene chemistry. The utilization of different furan derivatives allows to customize the coating properties due to the distinct chemical structure of the base monomers. Moreover, the incorporation of different thiols expands the range of achievable properties by manipulating the number of thiol-functionalities in the monomers involved in the network formation.

In our study, we focused on two specific furan derivatives, namely 2,5-Furandimethanol (FDM) and cis-cyclobutane-1,2-dicarboxylic acid (CBDA-2) as a starting platform for the synthesis of two new allylated monomers. Notably, the CBDA-2 derivative's high rigidity leads to an improved thermo-mechanical property, providing a promising avenue for tailoring coatings to specific applications.

In-depth investigations into UV-curing were carried out using FTIR and photo-rheology, demonstrating the excellent reactivity of the synthesized -ene monomers with commercial thiols. The achieved conversion rates were high, exceeding 70%, for all the investigated formulations. In addition, a range of thermo- and mechanical tests were conducted on the UV-cured coatings. The results revealed that the coatings exhibited comparable or even superior properties compared to previous studies in the

field. This highlights the potential of furan derivatives as a basis for green alternatives in coating applications.

In conclusion, this study successfully demonstrates the feasibility of developing new green alternatives based on furan derivatives in the field of coating applications. The combination of distinct furan derivatives and thiol functionalities allows for fine-tuning the coating properties to meet specific requirements. These findings can lead to further advancements in eco-friendly coatings and offer a sustainable approach to enhance material performance in various applications.

References

1. Isikgor, F. H. & Becer, C. R. Lignocellulosic biomass: a sustainable platform for the production of bio-based chemicals and polymers. *Polym. Chem.* 6, 4497–4559 (2015).
2. Gandini, A. Polymers from renewable resources: A challenge for the future of macromolecular materials. *Macromolecules* 41, 9491–9504 (2008).
3. Pezzana, L. *et al.* Thiol-ene biobased networks: Furan allyl derivatives for green coating applications. *Prog. Org. Coatings* 173, 107203 (2022).
4. Pezzana, L. Ferulic bio-based monomers for UV-curing. (2020).
5. Shukla, V., Bajpai, M., Singh, D. K., Singh, M. & Shukla, R. Review of basic chemistry of UV-curing technology. *Pigment Resin Technol.* 33, 272–279 (2004).
6. Kaur, M. & Srivastava, A. K. Photopolymerization: A review. *J. Macromol. Sci. - Polym. Rev.* 42, 481–512 (2002).
7. Lowe, A. B., Hoyle, C. E. & Bowman, C. N. Thiol-yne click chemistry: A powerful and versatile methodology for materials synthesis. *J. Mater. Chem.* 20, 4745–4750 (2010).
8. Bagheri, A. & Jin, J. Photopolymerization in 3D Printing. (2019) doi:10.1021/acsapm.8b00165.
9. Dickens, S. H., Stansbury, J. W., Choi, K. M. & Floyd, C. J. E. Photopolymerization kinetics of methacrylate dental resins. *Macromolecules* 36, 6043–6053 (2003).
10. Senyurt, A. F., Wei, H., Hoyle, C. E., Piland, S. G. & Gould, T. E. Ternary Thiol - Ene / Acrylate Photopolymers : Effect of Acrylate Structure on Mechanical Properties. 4901–4909 (2007).
11. Hoyle, C. E. & Bowman, C. N. Thiol-ene click chemistry. *Angew. Chemie - Int. Ed.* 49, 1540–1573 (2010).
12. Lowe, A. B. Thiol-ene 'click' reactions and recent applications in

polymer and materials synthesis. *Polym. Chem.* 1, 17–36 (2010).

13. Lee, Y., Kwon, E. E. & Lee, J. Polymers derived from hemicellulosic parts of lignocellulosic biomass. *Rev. Environ. Sci. Biotechnol.* 18, 317–334 (2019).

14. Giechaskiel, B. & Clairotte, M. Fourier transform infrared (Ftir) spectroscopy for measurements of vehicle exhaust emissions: A review. *Appl. Sci.* 11, (2021).

15. Petit, S. & Madejova, J. Fourier Transform Infrared Spectroscopy. *Dev. Clay Sci.* 5, 213–231 (2013).

16. Leyva-Porras, C., Cruz-Alcantar, P., Espinosa-Sol, V. & Saavedra-Leos, M. Z. Application of Differential Scanning Calorimetry (DSC) and Modulated Differential Scanning. *Polymers (Basel).* 12, 1–21 (2019).

17. Mettler Toledo. Thermal Analysis Excellence Differential Scanning Calorimetry for all Requirements Unmatched DSC Performance. 1–14 (2011).

18. Northrop, B. H. & Coffey, R. N. Thiol-ene click chemistry: Computational and kinetic analysis of the influence of alkene functionality. *J. Am. Chem. Soc.* 134, 13804–13817 (2012).

19. Pezzana, L. & Sangermano, M. Fully biobased UV-cured thiol-ene coatings. *Prog. Org. Coatings* 157, 106295 (2021).

20. Yoshimura, T., Shimasaki, T., Teramoto, N. & Shibata, M. Bio-based polymer networks by thiol-ene photopolymerizations of allyl-etherified eugenol derivatives. *Eur. Polym. J.* 67, 397–408 (2015).

21. Pezzana, L. Cross-Linking of Biobased Monofunctional Furan Epoxy Monomer. (2022).

Acknowledgments

I would like to express my heartfelt gratitude to my supervisor, Prof. Marco Sangermano, for providing me with the opportunity and support to conduct my thesis under his guidance. Marco, your mentorship and patience during these months have been truly precious. Your open-door policy, interest in my personal growth and wellbeing went beyond the academic boundaries, and I am grateful for that.

I also want to express a special thanks to Lorenzo for his passion and expertise, which served as a constant source of inspiration for me.

My deepest appreciation goes to my mom, Angela, for her endless love, patience, understanding, and encouragement. Your support has meant the world to me. Mamica, mulțumesc pentru tot.

This work is dedicated to the loving memory of my grandfather, bunelu Mihai, who instilled in me the passion for curiosity. The love for learning and appreciation of hard work comes from you. Although I will forever miss you, your love and kindness will continue to guide me in my life.

I want to express my heartfelt gratitude to my closest friends who have stood by my side and provided unwavering support throughout my journey. The road trips together, adventures we embarked on, the inside jokes we created, and the shared memories we hold close have taught me the profound value of friendship.

I would also like to thank all my office colleagues for the enriching daily discussions, delightful coffee breaks and shared moments that we enjoyed together, both inside and outside the lab. Your camaraderie and support have been an integral part of my experience, making the work environment not only productive but also enjoyable.

There are many others who have contributed to this phase of my life and deserve my appreciation. Although I cannot mention everyone individually, please know that none of you have been forgotten, and I am grateful for each one of you.